CrossMark

Future intensification of hydro-meteorological extremes: downscaling using the weather research and forecasting model

R. El-Samra[1] · E. Bou-Zeid[2] · H. K. Bangalath[3] · G. Stenchikov[3] · M. El-Fadel[1]

Abstract A set of ten downscaling simulations at high spatial resolution (3 km horizontally) were performed using the Weather Research and Forecasting (WRF) model to generate future climate projections of annual and seasonal temperature and precipitation changes over the Eastern Mediterranean (with a focus on Lebanon). The model was driven with the High Resolution Atmospheric Model (HiRAM), running over the whole globe at a resolution of 25 km, under the conditions of two Representative Concentration Pathways (RCP) (4.5 and 8.5). Each downscaling simulation spanned one year. Two past years (2003 and 2008), also forced by HiRAM without data assimilation, were simulated to evaluate the model's ability to capture the cold and wet (2003) and hot and dry (2008) extremes. The downscaled data were in the range of recent observed climatic variability, and therefore corrected for the cold bias of HiRAM. Eight future years were then selected based on an anomaly score that relies on the mean annual temperature and accumulated precipitation to identify the worst year per decade from a water resources perspective. One hot and dry year per decade, from 2011 to 2050, and per scenario was simulated and compared to the historic 2008 reference. The results indicate that hot and dry future extreme years will be exacerbated and the study area might be exposed to a significant decrease in annual precipitation (rain and snow), reaching up to 30% relative to the current extreme conditions.

Keywords Climate change · Complex topography · Extreme heat · HiRAM · Mediterranean · WRF

1 Introduction

In recent years, various regions have witnessed seasonal weather changes that were associated with negative environmental impacts and that led to socio-economic burdens across many countries. In addition, recent research indicates potentially greater changes in regional weather under future climate conditions (Sun et al. 2007; Brown et al. 2008; IPCC 2013). In particular, climate change has been reported to intervene with the frequency and intensity of extreme events (Christidis et al. 2005). Examples of such events are heatwaves, droughts, and floods that have adverse effects on important aspects of our society and economy, such as water resources, crop yield, and human health (Seneviratne et al. 2014). Therefore, understanding the vulnerability to climate change, and corresponding mitigation measures and adaptation strategies to potential negative impacts, became imperative at both regional and local levels. This is particularly important in order to capture extremes that are highly variable in space and time and are not adequately simulated by global climate models (GCMs). This necessitates the use of regional climate models (RCMs) to downscale the large-scale forecasts from GCMs (Barrera-Escoda et al. 2014). Downscaling is particularly needed in regions with complex topographies that cannot be resolved by coarse GCMs.

Downscaling can be conducted through various techniques that can be mainly categorized into two groups

✉ M. El-Fadel
mfadel@aub.edu.lb

[1] Department of Civil and Environmental Engineering, American University of Beirut, Beirut, Lebanon

[2] Department of Civil and Environmental Engineering, Princeton University, Princeton, NJ, USA

[3] King Abdullah University of Science and Technology, Thuwal, Saudi Arabia

known as dynamic and statistical downscaling (Evans et al. 2012). The latter generates semi-empirical relationships between local and large-scale climate based on statistical methods (Wilby et al. 1998; Flaounas et al. 2013b). It requires less computational power but is constrained by the hypothesis of stationarity in the associations between local observations and simulated climate, which are developed for the present and then applied in a future variable climate (Diaz-Nieto and Wilby 2005). Dynamic downscaling, used in this study, consists of driving an RCM at high resolution by the output of an atmospheric high resolution GCM for the region of interest (Wang et al. 2004). They produce an accurate regional climate with fine-scale topographies that are lacking in the GCMs (Antic et al. 2004). Dynamic downscaling is computationally demanding and needs substantial implementation effort, but a crucial appeal of the technique is the reliance on physical processes rather than statistical relationships, relaxing the need for assuming stationarity (Fowler et al. 2007). The high resolution over a limited region permits improved depiction of basic surface forcings such as topography, shorelines, inland water or land-surface features and heterogeneity (Giorgi and Mearns 1991).

Some recent RCM downscaling studies attempted to examine the change in the mean and extreme climate variables (temperature, precipitation, etc.) (Cardoso et al. 2012; Gao et al. 2012; Warrach-Sagi et al. 2013). These parameters can be highly affected by regional variability, especially in regions with complex topography. The use of high-resolution RCMs in such intricate domains usually improves the average annual precipitation and mean temperatures fields in comparison with the driving GCM when simulations are conducted over a time span of multiple consecutive years (Salathé et al. 2008; Caldwell et al. 2009), but their added value for capturing extremes is not well documented. In addition, when the grids of RCMs become finer than 10 km, which is needed over complex terrain but necessitate smaller time–steps, the simulations become very demanding computationally with little to no feasibility to perform downscaling for multiple decades that are usually simulated by GCMs. Therefore, increased spatial resolution invariably comes with the caveat of reduced temporal (as well as spatial) coverage. If the aim is to understand the vulnerability of a region to climate change, one must therefore judiciously select future periods to downscale using RCMs. These two challenges, namely the complex topography requiring dynamic downscaling and the need to select carefully future periods to downscale, frame the scope of this study. Such challenges are eminently represented in the eastern Mediterranean basin where temperature and precipitation are sensitive to orographic elevation changes that occur at spatial scales much smaller than the grid scale of a GCM. Furthermore, weather and climate variability on

weekly to yearly scales implies that severe adverse impacts of climate change are localized in time, which implies that the periods when such impacts occur need to be identified for downscaling based on GCM data.

This study aims to assess the value, and investigate the challenges, of regional dynamic downscaling in topographical complex regions during extreme periods. As a pilot area, we selected the country of Lebanon. With its location in the temperate zone along the eastern Mediterranean and its complex topography where two mountain ranges run parallel to the coast and amplify the impact of the Mediterranean Sea on the climatology of the coastal and interior regions (Atlas Climatique du Liban 1977). It is a representative example of a location where dynamic downscaling is expected to be challenging, yet valuable. The objectives of the study are (1) to propose a method whereby only extreme years are identified and selected for downscaling to gage the worst-case impacts (in this paper we focus on dry and hot years) of climate change; (2) to dynamically downscale global climate predictions for these extreme years to a local scale using the Weather Research and Forecasting (WRF) model (Skamarock et al. 2008) forced by the High Resolution Atmospheric Model (HiRAM) (Zhao et al. 2009; Jiang et al. 2012) for the past (as a reference) and the future; and (3) to generate information on the small-scale spatial variability of vulnerability that cannot be captured by coarse GCM simulations. The novelty of the contribution centers on (1) the selection of "crucial-periods" for targeted downscaling using anomaly scores that can be defined to reflect any variable of interest, and (2) the focus on the value of downscaling for capturing extremes and corresponding statistics as proxies for the magnitude of the most severe climate change impacts. Beyond methodological contributions, the implications of the results on water resources are valuable given that the overall region is already water stressed and continues to suffer from socio-political conflicts coupled with a lack of integrated water management policies (Bou-Zeid and El-Fadel 2002).

2 Methods and data

2.1 Global model

HiRAM is a global atmospheric model that was developed by the Geophysical Fluid Dynamics Laboratory (GFDL) to be applicable to a broad range of resolutions (Chen and Lin 2011). It was developed based on the standard version of GFDL atmospheric GCM (AM2) (Zhao et al. 2009) with 32 vertical levels (instead of the 24 levels in AM2) to provide refined vertical resolution particularly near the tropopause (Jiang et al. 2012). HiRAM also uses a cubed-sphere

Table 1 Global climate models assessed, in order of decreasing resolution

Model name	Institution	Horizontal grid	References
GFDL-HiRAM-C360	NOAA Geophysical Fluid Dynamics Laboratory	25×25 km	Delworth et al. 2006; Donner et al. 2011
CCSM4	US National Centre for Atmospheric Research	100×117 km	Gent et al. 2011
HadGEM2-AO	National Institute of Meteorological Research/Korea Meteorological Administration	208×117 km	Collins et al. 2011; Martin et al. 2011
INM-CM4	Russian Institute for Numerical Mathematics	222×140 km	Volodin et al. 2010
MRI-CGCM3	Meteorological Research Institute	320×160 km	Yukimoto et al. 2011

Note that the area of the study area is 10,452 km^2, which implies that HiRAM is the only GCM that has more than one grid cell over the country

application of a finite-volume dynamic core and is linked to GFDLS's new land model (LM3) (Donner et al. 2011).

The model has been used in studies of hurricane inter-annual variability, multi-decadal trends, responses to 21st-century warming, and seasonal hurricane predictions for the North Atlantic and East Pacific (Zhao and Held 2010; Zhao et al. 2010; Jiang et al. 2012). Gall et al. (2011) investigated its potential as a forecasting tool for the near-term and for intra-seasonal hindcasting of tropical cyclones in the Atlantic basin from 2006 to 2009, demonstrating skilled near-term forecasts of cyclones track and intensity about their respective benchmarks. Another study by Chen and Lin (2011) used HiRAM to predict the tropical cyclone activity in the North Atlantic basin at 25 km resolution and reported a high correlation coefficient (R^2) of 0.96 between observed and simulated hurricane counts for the 2000–2010 seasons.

In this study, HiRAM is used at a horizontal grid spacing of 25 km (Bangalath and Stenchikov 2015) to simulate historic (1975–2004) and future (2007–2050) stages using both Representative Concentration Pathways (RCP) 4.5 and 8.5 scenarios.[1] The sea surface temperatures, completed for the International Panel for Climate Change Assessment Report AR5 project, were adopted from the GFDL Earth System Model runs as the bottom boundary conditions over water surfaces. Recommended time-varying greenhouse gas and stratospheric/tropospheric aerosol distribution datasets were used to reproduce the observed radiative forcing in the model (Bangalath and Stenchikov 2015).

To evaluate the selected driving GCM (HiRAM), data from five other global models selected to have a range of resolutions (Table 1) forced by RCP4.5 and 8.5 were obtained from the Coupled Model Intercomparison Project phase 5 (CMIP5) archive (https://pcmdi9.llnl.gov/projects/esgf-llnl/) (Taylor et al. 2012). Then, yearly median

temperature and annual accumulated precipitation time series over Lebanon (which is smaller than one grid cell in all models except HiRAM) were generated for each GCM for the period 2007–2050 to compare their simulated average decadal climatology in the study region for both scenarios. The median, minimum and maximum values for each decade GCM of the yearly averaged temperature and yearly accumulated precipitation are compared in Fig. 1. HiRAM has the highest resolution (25 km) of all models used and its predicted precipitation for the past period 2007–2010 is the closest to the average annual precipitation of 700 to 800 mm in the study area (Atlas Climatique du Liban 1977). The decreasing precipitation trend in HIRAM for the future is more pronounced than the other models. The lower resolution models produce lower rainfall for 2007–2010, which might be expected given their limitation in resolving the complex topography in the study area that plays a significant role in inducing orographic precipitation. On the other hand, HIRAM has a cold bias for the median annual temperature (for 2007–2010) for both RCPs, whereas HadGEM2-AO and CCSM4 produce the ≈20 °C mean temperature over the study area (Atlas Climatique du Liban 1977) more accurately. We opted for HiRAM forcing to drive WRF in this study because (1) our simulations suggest that WRF can correct some of the temperature biases it inherits from its forcing model (El-Samra 2016) and therfore the cold bias of HiRAM is less of a concern, (2) the focus is primarily on precipitation and on the hydrologic impacts of climate change that are captured well by HiRAM, and (3) the high resolution of HiRAM allows a start with a coarse grid of 9 km in WRF (rather than 27 km for example). However, we note that demonstrating a higher performance of a GCM in simulating present-day climate may not be a sufficient indicator of the performance for future climate (Christetin and Christenin 2007); this is a limitation that cannot be overcome. Moreover, to further reduce the impact of GCM bias on climatic trends, we select the historic baseline for the hot and dry year from the RCP4.5 simulation of HiRAM to assess future climates trends, instead of relying on observations or reanalyses.

---

[1] RCP 4.5 reflects a stabilization scenario where total radiative forcing plateaus before 2100 by the utilization of a variety of technologies and strategies for reducing GHG emissions (Clarke et al. 2007). As for RCP 8.5, it is characterized by increasing GHG emissions over time, leading to high GHG concentrations (IPCC 2013).
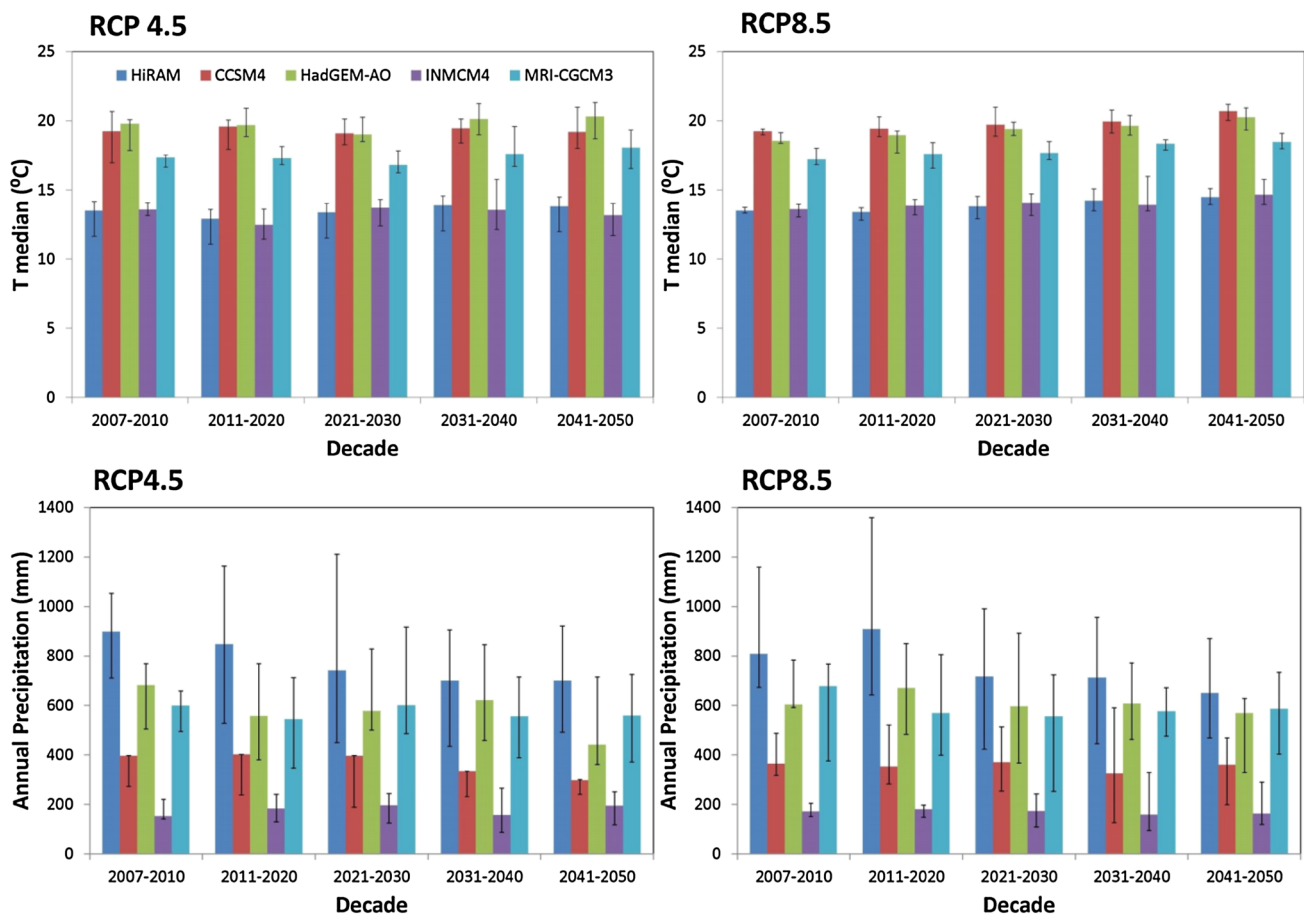
Fig. 1 Average decadal climatology over study area from five GCMs. (*up*: yearly median, minimum and maximum temperature for every GCM during each decade; *down*: yearly accumulated, minimum and maximum precipitation for every GCM during each decade)

2.2 Regional model

The regional model used for this study is WRF, with the Advanced Research (ARW) dynamics solver, version 3.4.1 (Skamarock et al. 2008). WRF is a non-hydrostatic three-dimensional atmospheric model suitable for both operational forecasting and atmospheric research applications (Heikkila et al. 2011). It accesses various databases directly to obtain information on terrain elevation, land cover and land use from the United States Geological Survey (USGS) and from the Moderate Resolution Imaging Spectroradiometer (MODIS) (Friedl et al. 2001) at various resolutions. These data cover the whole earth surface at a finest resolution of 30 s in both latitudinal and longitudinal directions, which corresponds to about 1 km at mid-latitudes.

WRF as an RCM was recently evaluated in several studies, which documented very good skill in simulating regional weather and climate (Lo et al. 2008; Bukovsky and Karoly 2009; Caldwell et al. 2009; Qian et al. 2010; Lebeaupin Brossier et al. 2011; Cardoso et al. 2012; Talbot et al. 2012; Flaounas et al. 2013a, b; Warrach-Sagi et al.

2013; Ramamurthy et al. 2015). A regional high resolution is achieved in the current simulations by using two one-way nested domains (Fig. 2a), with 9 and 3 km horizontal resolutions. The highest resolution of 3 km was shown to be sufficient in previous tests comparing historic WRF simulations over the study area to a wide array of ground observations; no significant improvement was noted when the resolution was further increased to 1 km (El-Samra 2016). The outer integration domain covers 1350×1700 km encompassing the eastern Mediterranean, to guarantee that synoptic-to-mesoscale systems that affect the coast of the study area are resolved in WRF. The inner domain extends over 462×579 km. MODIS (for the year 2001) land use data was used with 21 land categories and Lambert Conformal projection (most convenient for mid-latitude regions since it yields a nearly uniform grid spacing). The time step used was 30 s for the largest domain, and all domains had 28 vertical levels (with a vertically-stretched grid) arranged according to terrain following hydrostatic pressure coordinates. The number of vertical levels is also based on the tests for historic periods conducted in El-Samra (2016).

Fig. 2 a WRF's two domains (9:3 km) configuration with a *color map* of terrain height above sea level (ASL) (m), **b** study area divided into five geo-climatic regions
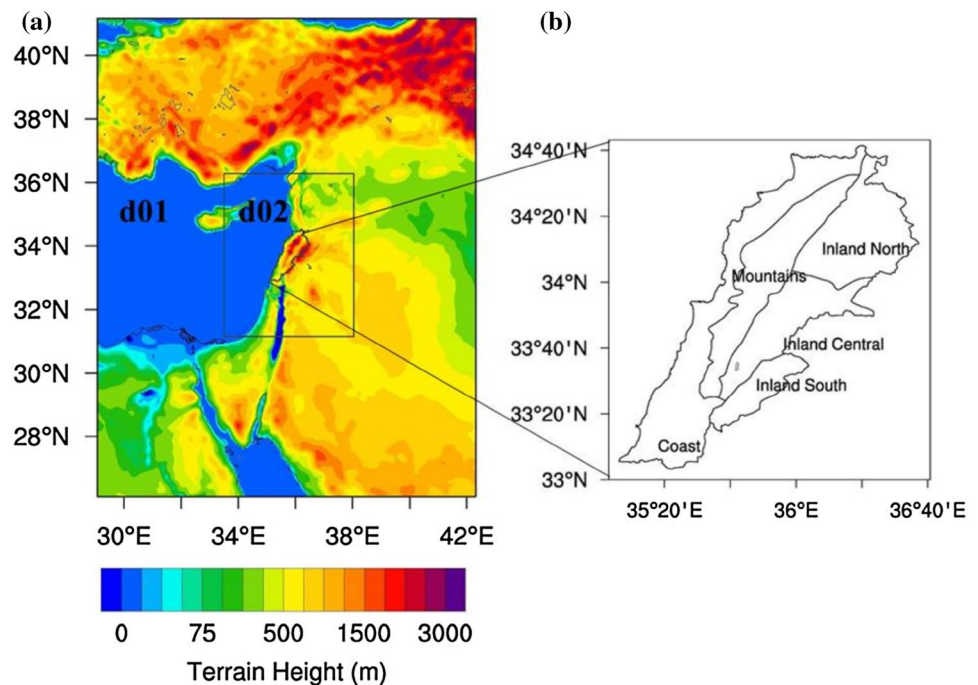
Initial and boundary conditions were obtained from HiRAM's past and future simulations. The time interval of the boundary data is 6 h, and the sea surface temperature (SST) was also updated every 6 h. WRF Preprocessing System (WPS) was used to interpolate HiRAM's output into WRF domains. Eight yearly downscaling simulations were performed to generate extreme future climate projections over the project area, four from RCP 4.5 and four from RCP 8.5 (one year per decade from each scenario from 2011 to 2050). In addition, two past years forced by HiRAM were also simulated to evaluate the model's ability to capture the cold and wet (2003) as weel as hot and dry (2008) extremes. The simulation of 2008 from RCP4.5 was then used as the historic baseline for inferring the future trends of the hot and dry extremes; this reduces the impact of GCM bias on the climatic trends. Each simulation covered a 13-months physical period, initialized on the first of December of the year preceding the year of interest to allow a one month spin-up period, which was discarded before analyzing the simulation data from January to December of the year of interest (Zhang et al. 2009; Gao et al. 2012; Soares et al. 2012).

Another key step in the model setup involves selecting the parameterization schemes. WRF has multiple options for parameterizing the physics of unresolved processes, as well as various schemes for the numerical discretization of the governing equations (Skamarock et al. 2008). In this work, the parameterizations schemes adopted are: WRF Single-Moment 6-Class Microphysics Scheme (WSM6) (Hong and Lim 2006), Monin Obukhov and Mellor Yamada Janjic (Eta) for surface layer and PBL physics (Mellor

and Yamada 1974; Janjic 2001), Rapid Radiative Transfer Model (RRTM) (Mlawer et al. 1997) and Dudhia Long Wave and Short Wave (LW/SW) for radiative processes (Dudhia 1989), and Noah Land Surface Model (LSM) (Chen and Dudhia 2001) for surface processes. The selection is based on our previous WRF tests as detailed in Talbot et al. (2012) and Li et al. (2013). The same WRF configuration used here also performed well in historic simulations over the study area forced by reanalyses data from GFS (El-Samra 2016). We modified the atmospheric equivalent CO_2 concentration in each simulated year of WRF to match the respective scenarios RCP4.5 and RCP8.5 and to be consistent with HIRAM. This alters the radiative balance of the simulations slightly but has a minor impact on the relatively short-term regional simulations we conduct with WRF (this was verified by comparing to simulations with current CO_2 concentration).

2.3 Selection of downscaling periods

The influence of global warming on the project area can be assessed by comparing past and future statistics of various meteorological fields from years selected to have extreme hydro-meteorological events such as heat waves, intense storms, or drought periods. Such events pose particular challenges for dynamic models and significant hazards for the affected areas. Therefore, our downscaling simulations do not aim to reproduce decadal-means or average climatological conditions, the trends of which are reasonably captured by GCM outputs despite their shortcomings. Our focus is rather on extreme years where the impacts
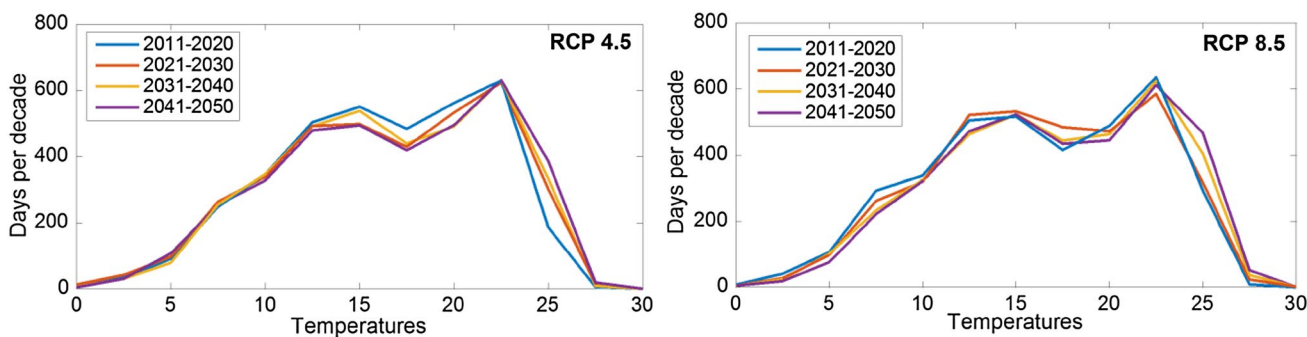
Fig. 3 Probability density functions of daily air temperatures (°C) at a coastal location near the city of Beirut (BIA station, detailed in Sect. 2.4) from the time series of HiRAM, for the 4 future decades

are the largest. Since these extreme years will be the tail of the decadal probability distribution functions (PDFs) for the various variables, a pertinent question is how representative are these tails of the general changes in these distributions. To address this question we plot in Fig. 3 the PDFs of 2 m air temperature at a coastal location near the capital Beirut simulated by HiRAM, for each decade separately. The PDFs depict a consistent monotonic decrease in the frequency of low and intermediate temperatures, and an increase in the frequency of the highest ($\geq$25 °C) temperatures. We also computed the mean and standard deviations for all decades and this shift seems to emanate from a shift in the mean, rather than a change in the variance. The figure also indicates that the PDFs, computed based on a decade of daily data, are sufficiently converged so that the changes at the tails are not random, but rather consistent and representative of overall changes in the PDF. This indicates that investigating the tails is justified and indeed beneficial for our purposes since we intend to focus on extreme events.

To identify such extreme years, the following procedure is adopted:

– Analyze HiRAM temperature and precipitation output time series for the "past" (2000–2010) and for the "future" (2011–2050 for RCP 4.5 and 8.5) (Fig. 4)
– Quantify the accumulated annual precipitation and the median temperatures for each year from 2000 till 2050.
– Select the two extreme years for the past (a cold and wet year, and a hot and dry year) and eight years in the future (only hot and dry years, one year per scenario per decade) based on the following anomaly score:

$$\text{Anomaly Score} = \frac{1}{2}\left(\frac{P_i - P_i}{\max(P_i - P_i)} + \frac{-(T_i - T_i)}{\max(T_i - T_i)}\right), \tag{1}$$

where P_i is the cumulative precipitation for year i (averaged over the domain of interest); $\langle P_i \rangle$ is the decadal-average (e.g. from 2021 to 2030) of the yearly precipitations P_i; T_i is the yearly median temperature (over the domain of interest); and $\langle T_i \rangle$ the decadal-average of the median temperatures T_i. The domain of interest here was taken as an area of 28917 km^2, spanning multiple HiRAM grid cells and fully encompassing the study area. The resulting minimum negative score corresponds to the critical/worst hot and dry year of the decade, while 2003 had the largest positive score in the historic decade. While we only focus on hot and dry future years, WRF historical simulations were performed for hot and dry as well as cold and wet years to "measure" the sensitivity of complex regions like the study area to extreme climate variability at both ends of the PDF.

The above process resulted in the selection of the following years: (1) 2003 as past cold and wet year and 2008 as past hot and dry year; (2) 2020, 2029, 2040 and 2050 as future dry and hot years from RCP4.5; and (3) 2017, 2023, 2035 and 2050 as future dry and hot years from RCP8.5. Figure 4 indicates that the precipitation variability is larger than the variability of the median temperature, and thus dominated the anomaly score. Another formulation can be adopted (with weight) but in this study we focus on precipitation extremes and as such this score is well suited for our purposes. It is important to mention that the anomaly score gave years 2011 in RCP4.5 and 2015 in RCP8.5 as the extreme years for the decade 2011–2020, but we opted not to simulate any additional actual past or current years other than 2003 and 2008 (although 2011 and 2015 are future years in the HIRAM simulation). Hence, we selected the second worst extreme years (2020 in RCP4.5 and 2017 in RCP8.5). This had some influence on the trends we will show later, but does not alter the general conclusions we make.

It is noteworthy that the simulated weather is a possible future realization, and unlikely to be the actual one

Fig. 4 HiRAM RCP4.5 and 8.5 annual cumulative precipitation (mm) and median temperature (°C) time series (2007–2050) over the study area (Lebanon)
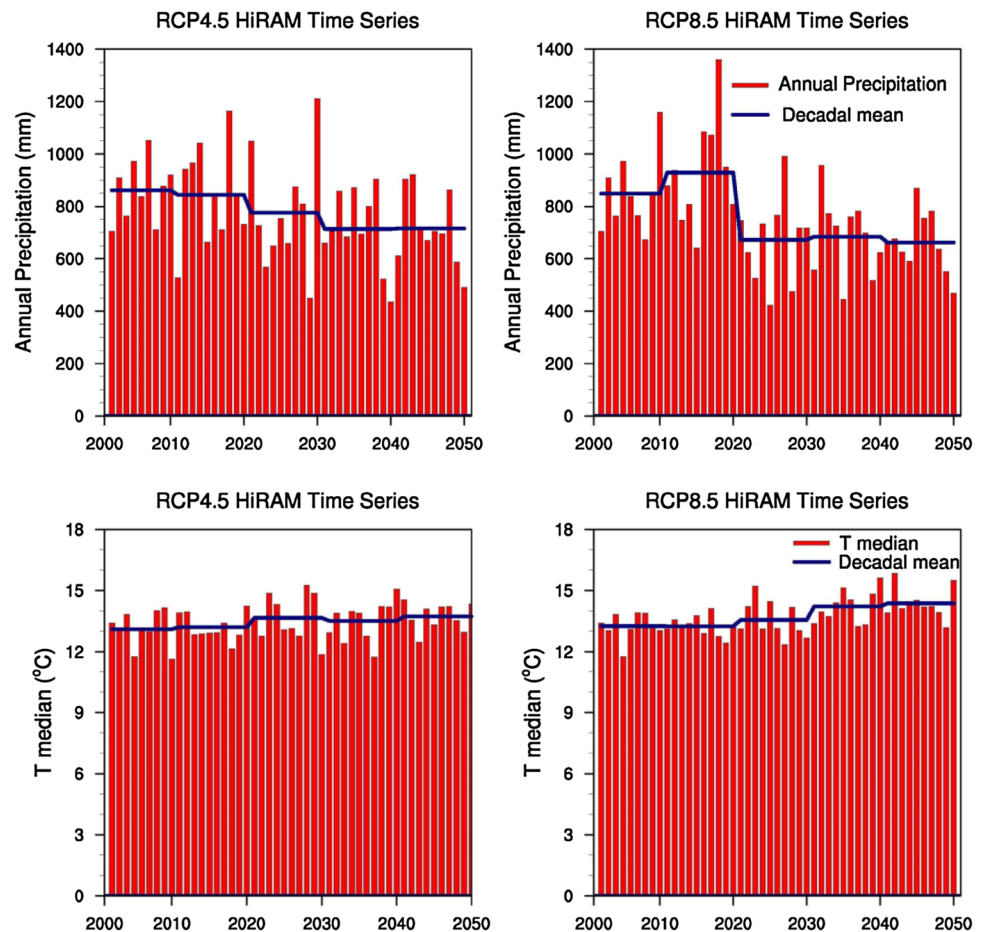
that is going to occur. Hence, the driest year forecasted by a GCM for the 2030–2040 decade, for example, might not be the actual driest year that will happen in that decade, but should be statistically representative of the actual driest year given that the PDFs seem reasonably converged as illustrated in Fig. 3.

2.4 Observational data

Before using any RCMs or mesoscale models for high-resolution future projections, it is critical that model outputs be assessed against historical observational data to evaluate their consistency in predicting spatial and temporal distributions (Laprise 2008). We assessed the use of WRF forced by meteorological reanalyses from the same region (El-Samra 2016), with very satisfactory results. We also perform a limited assessment of HiRAM/WRF in this paper. To that end, comparisons between simulated and observed 2 m temperatures and rainfall climatologies were conducted. WRF dynamical downscaling monthly results for rainfall and temperature from past simulations (2003 and 2008, the two extreme years for that decade according to HiRAM) are compared with monthly observational datasets from weather stations that have continuous data for the decade of 2000–2010 across the project area. These tests will show if the dominant temporal features (magnitude, spatial pattern, and monthly variations) of rainfall and temperature, and their ranges, are well captured by HiRAM/WRF runs at various spatial locations, and will guarantee that the HiRAM/WRF extreme variability is within the observed variability for historical periods.

To identify the spatial and temporal climatic data that can be used, a review and assessment of the quality, comprehensiveness and span of several climatic data sources was undertaken. Based on a long-term trend of weather parameters including temperature, relative humidity, rainfall and wind, the Atlas Climatique du Liban (1977) divides the project area into three broad climatic trends: the coastal, the mountainous, and the inland, each of which is further subdivided into sub-regions. We found that the subregional divisions are only significant in the present analyses for the inland zone, which is partitioned into the north, central and south sub-regions based on the difference in annual precipitation (Fig. 1b). Continuous observations with complete monthly data were assessed from available stations for the five geo-climatic regions.

Fig. 5 Annual mean temperature (°C) (**a**) 2003 HIRAM; (**b**) 2003 WRF 3 km resolution; (**c**) 2008 HiRAM; (**d**) 2008 WRF 3 km resolution. The locations of the 3 observational stations used in the assessment are also shown
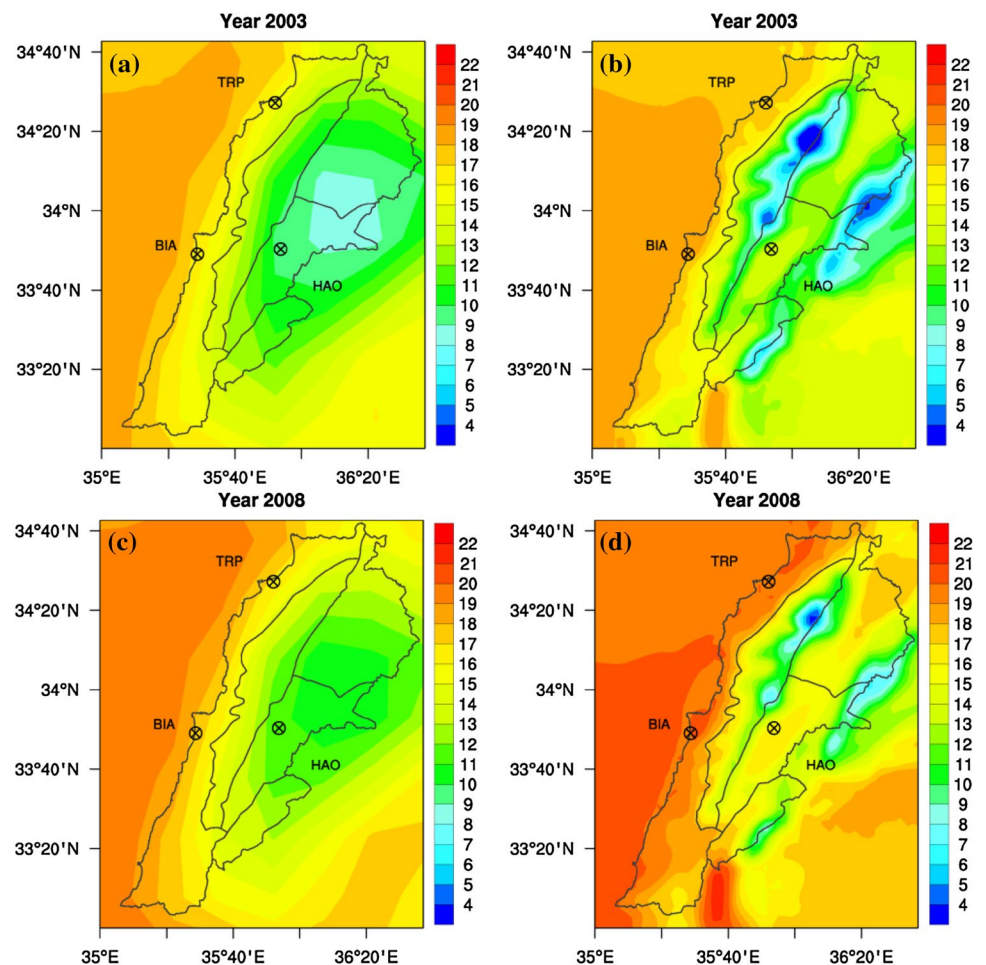
Data were available through the website TuTiempo.net.,[2] which compiles and stores data from meteorological stations around the world. Only three stations were found to have continuous daily data for temperature and rainfall for the period 2000–2010, two (BIA and TRP) located along the coastal zone and one located in the central inland region (HAO). Moreover, the anomaly score in Eq. (1) was used to determine the two past extreme years (wet/cold and dry/hot) in the observational data during the period 2000–2010 at each of the three stations (BIA, TRP and HAO). The monthly outputs of WRF and HiRAM are then compared to the observed yearly-averaged temperature and yearly-accumulated precipitation statistics (average over the decade, minimum, and maximum), as well as to the same observed variables in the two observational extreme years. Note that the evaluation did not cover snow fall because no records were available for this variable in the study area.

3 Results and discussion

In this section, we will first assess the results from HiRAM/WRF against historical observational data for 2 m temperature and accumulated annual precipitation in order to evaluate the model's consistency in predicting spatial and temporal distributions of these variables. Next, the possible influence of climate change impacts on the study area are inferred by comparing past and future precipitation statistics from WRF simulations driven by HiRAM. The comparison is also extended to cover climate indices related to precipitation over the study area. We reemphasize that in the case of presence of biases in precipitation or temperature from WRF runs, which can originate both from HiRAM and WRF simulations, one can expect the biases to have a moderate influence on the difference fields (the anomalies) since they would be comparable in past and future HIRAM/WRF runs.

3.1 Recent historic extreme years (2003 and 2008)

3.1.1 Temperature

Figure 5 illustrates the annual mean temperature maps during 2003 and 2008 for the study area resulting from HiRAM and WRF simulations. HiRAM alone identifies the large-scale distribution of mean annual temperature but misses to reproduce the local topographies well. The figure obviously replicates the close relationship between altitude and temperature and shows that the finer resolution WRF simulations are superior in capturing the temperature changes
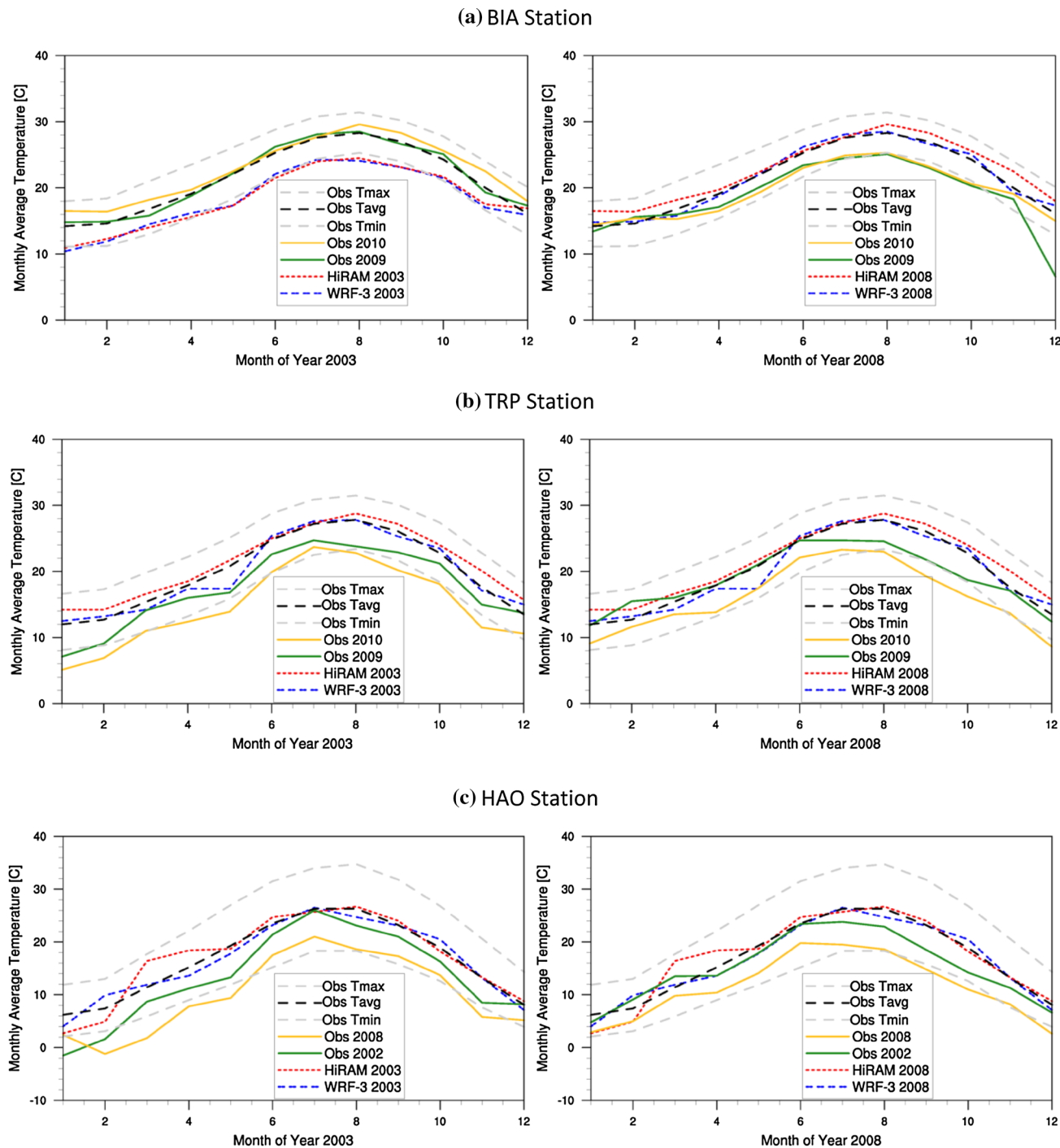

(a) BIA Station

(b) TRP Station

(c) HAO Station

Fig. 6 Simulated (WRF-3 and HiRAM) monthly average 2 m temperature (°C) for years 2003 and 2008 in comparison to observed decadal monthly average, maximum and minimum (2000–2010) and observed monthly average values for the extreme years 2009 and 2010 for BIA and TRP, and 2002 and 2008 for HAO

related to elevation in the mountain ranges, alongside the coast and in the inland regions. For instance, the northern inland semi-arid region located between two mountain ranges is delineated very well by WRF, while HiRAM's coarse resolution completely misses it. In addition, HiRAM missed many regional details such as the low temperature in the west mountain ranges: the minimum temperature is simulated approximately 0.8° to the east compared to WRF. WRF reproduces the spatial configuration of temperature variability skilfully, as well as the gradient of the temperature variability that is higher at high altitude and lower near sea levels. Therefore, WRF captures the regional temperature differences between the cold (2003) (Fig. 5b) and hot (2008) (Fig. 5d) simulated extreme years reasonably well.

In order to evaluate the model's skill in capturing the temperature variability over the study area, we calculated the simulated average monthly temperatures (T) [and Precipitations (P) in the next subsection] during 2003 and 2008 for the three weather stations considered, where the model data at the location of each station was used (Fig. 5). For observation data of each station, the mean values for each month were averaged over the 11 available years (each

month separately, from 2000 till 2010) for observed temperature and accumulated precipitation. The average over a given month across all years, as well as the average for the whole 11 years, were then also calculated. In addition to the monthly average over all years, the maximum and minimum monthly-mean values of T and P were computed for each month over the 11 years from the observations for the whole decade (e.g. hottest July in these 11 years). The simulated monthly mean temperature for 2003 and 2008 were then compared to observed ranges to check if WRF outputs are within these ranges for T and P. As previously noted, the observational data were for the observed extreme years (wet/cold and dry/hot) determined from the application of the anomaly score to the observational time series from 2000 to 2010. It is worthwhile to mention that the anomaly score resulted in the same past observed extreme years at both coastal stations (BIA and TRP) (2009 as wet/cold year and 2010 as dry/hot year); however, these years were different at the inland station (HAO) (2002 as wet/cold year and 2008 as dry/hot year) (Fig. 6).

Based on the evaluation for the three stations for the years 2003 and 2008, we found that the average temperate

Fig. 7 Annual precipitation (mm) (**a**) 2003 HIRAM 25 km resolution; (**b**) 2003 WRF3 km resolution; (**c**) 2008 HiRAM 25 km resolution; (**d**) 2008 WRF 3 km resolution The locations of the 3 observational stations used in the assessment are also shown
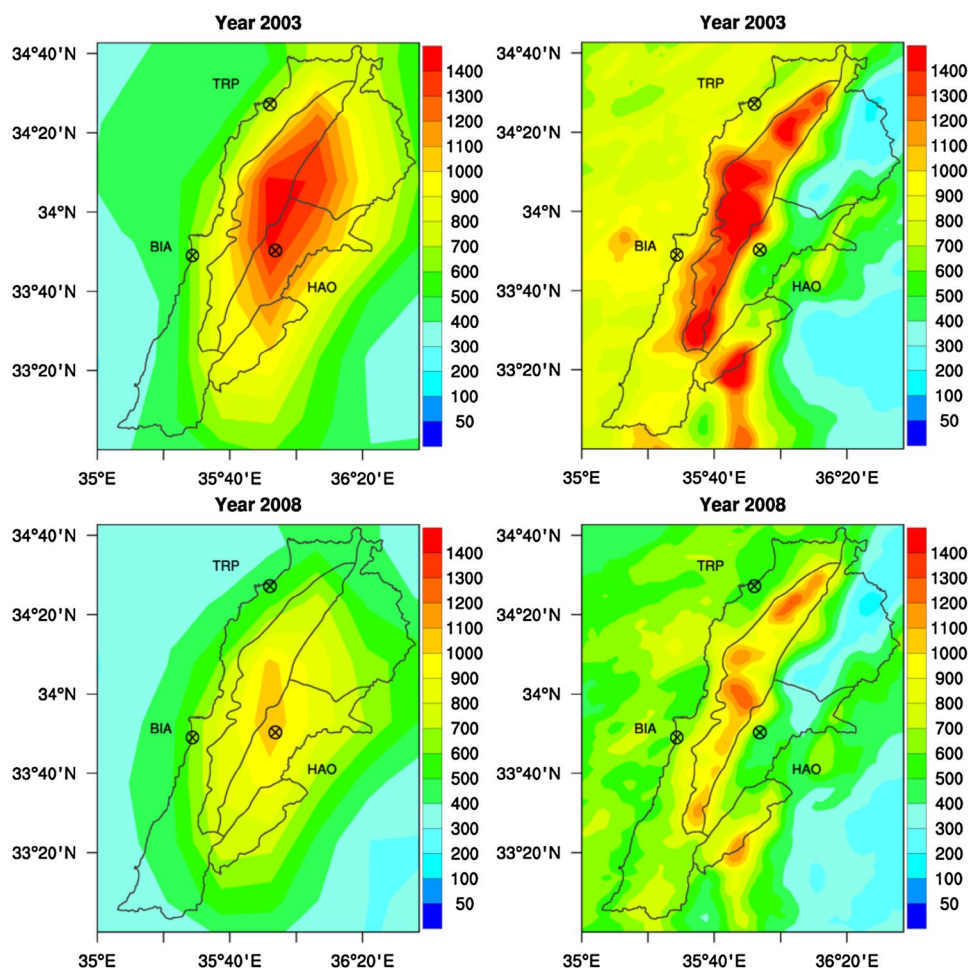
outputs of WRF 2003 and 2008 fall in the observed climatological ranges better than HiRAM's monthly simulated temperatures. Except for BIA, which is influenced by the proximity to the sea (recall the sea surface temperature is the same in WRF and HiRAM), WRF produces warmer temperatures than HiRAM, and is closer to the observed

averaged temperatures. The downscaling thus corrects some of the cold bias it inherits from HiRAM. However, some cold-bias persists; for example, both models indicate low average monthly temperatures for January at all three stations that are below the observed Tmin (which represents the coldest observed January for 2000–2010) by
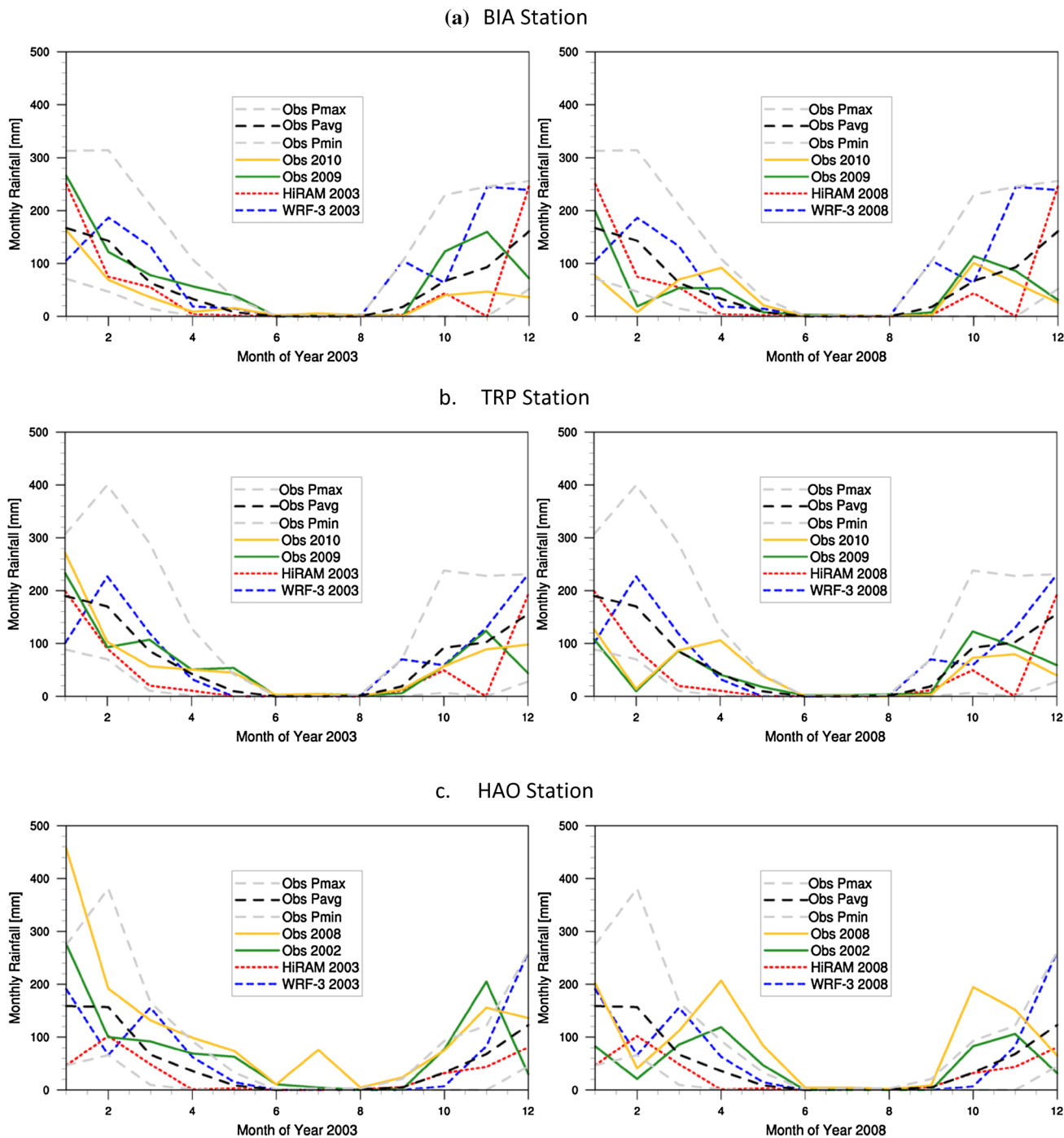

Fig. 8 Simulated (WRF-3 and HiRAM) monthly accumulated rainfall (mm) for years 2003 and 2008 in comparison to observed decadal monthly average, maximum and minimum (2000–2010) and observed monthly average values for the extreme years 2009 and 2010 for BIA and TRP, and 2002 and 2008 for HAO

1–3 °C. These biases underline the difficulties for temperature simulations over complex topographical regions, even for the high-resolution WRF simulations. For other months, however, the WRF simulations are within the range of observations, indicating that the simulations are reasonable depictions of the climate. This might suggest that the bias in January in WRF is related to the 1-month warm-up, and potentially with a longer initialization from HiRAM, better results could be obtained. The variability at the sub-yearly time scale (differences between the hottest and coldest month) are captured well. The inter-annual variability, on the other hand, cannot be assessed since we would need to simulate all 11 years with WRF to attain the same level of variability. The selection of 2003 and 2008 based on our anomaly score, which is also influenced by precipitation, does not guarantee that they represent the hottest and coldest years to capture the inter-annual variability.
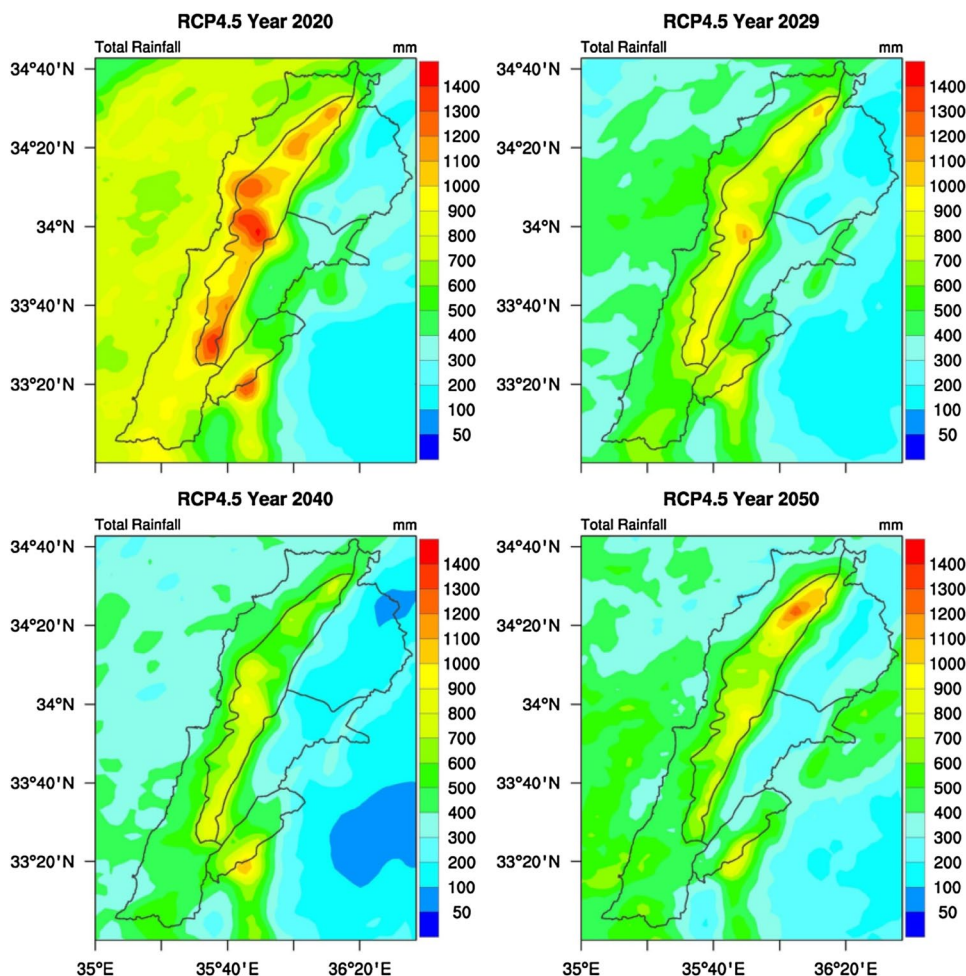
3.1.2 Precipitation

The wet season in the study area takes place primarily between the months of November and April with interspersed wet days through September–October and May, when precipitation is influenced by the influx of humid air

Table 2 Annual precipitations (mm) for HiRAM and WRF over the study area

Model	Reference	RCP4.5				RCP8.5			
	2008	2020	2029	2040	2050	2017	2023	2035	2050
HiRAM	711	732	450	436	491	1072	526	445	468
WRF (total)	710	738	538	440	494	887	553	498	582
WRF (rain)	662	681	469	368	471	771	521	452	552
WRF(snow)	48	57	69	72	23	116	32	46	30

Fig. 9 RCP4.5 accumulated rainy-season rainfall (mm) for the extreme years (hottest and driest per decade) under consideration

from the Mediterranean sea. The orographic features control precipitation: when this moist air reaches the coast from the west, it is uplifted by the mountains and then cools and condenses. Precipitation upsurges on the windward slopes and diminishes on the leeward inclines (since the air starts warming as it descends and the relative humidity decreases), creating a band of high annual precipitation parallel to the seaward slope of the west mountain range and along the coastal area. The average annual rainfall in the coastal zone ranges between 500 and 1100 mm, whereas the average annual precipitation over the mountainous region varies between 900 and 1850 mm (Atlas Climatique du Liban 1977; Akadan 2008).

The high spatial resolution of the RCM is central to simulating mesoscale phenomena and adding value to the GCM. For instance, Leung and Qian (2003) revealed considerable enhancement in the simulation of precipitation for the Pacific Northwest following the decrease in grid cell size of an RCM. As mentionaed above, the present model set-up is able to resolve the high resolution structure of storms and their impacts on precipitation in complex

topographies, and this is illustrated for both wet (2003) and hot (2008) extreme years in Fig. 7. WRF reproduces the very high precipitation over the western mountains and the high precipitation over the coast while the GCM misses most of the fine-scale details due to its coarse resolution.

The monthly rainfall comparison for the three observational weather stations shows that WRF provides more realistic simulations of recent climatology than HiRAM (Fig. 8). For all stations considered, WRF shows a good representation of seasonal and geographic distribution of rainfall: the effect of the main geographical features (coastal and inland) is captured, along with the reproduction of the seasonal cycle. As expected, coarse resolution models miss some of the spatial patterns and can produce significant discrepancies (for example HiRAM in 2008 at the inland HAO station), which WRF can correct.

The overall comparison between past regional model results and weather station data is quite reasonable. Recall that there is no reason to expect WRF to reproduce exactly the 2000–2010 observed average at any station, but it is anticipated to be withing the observational range.

Fig. 10 RCP4.5 accumulated rainy-season snowfall (mm) for the extreme years (hottest and driest per decade) under consideration
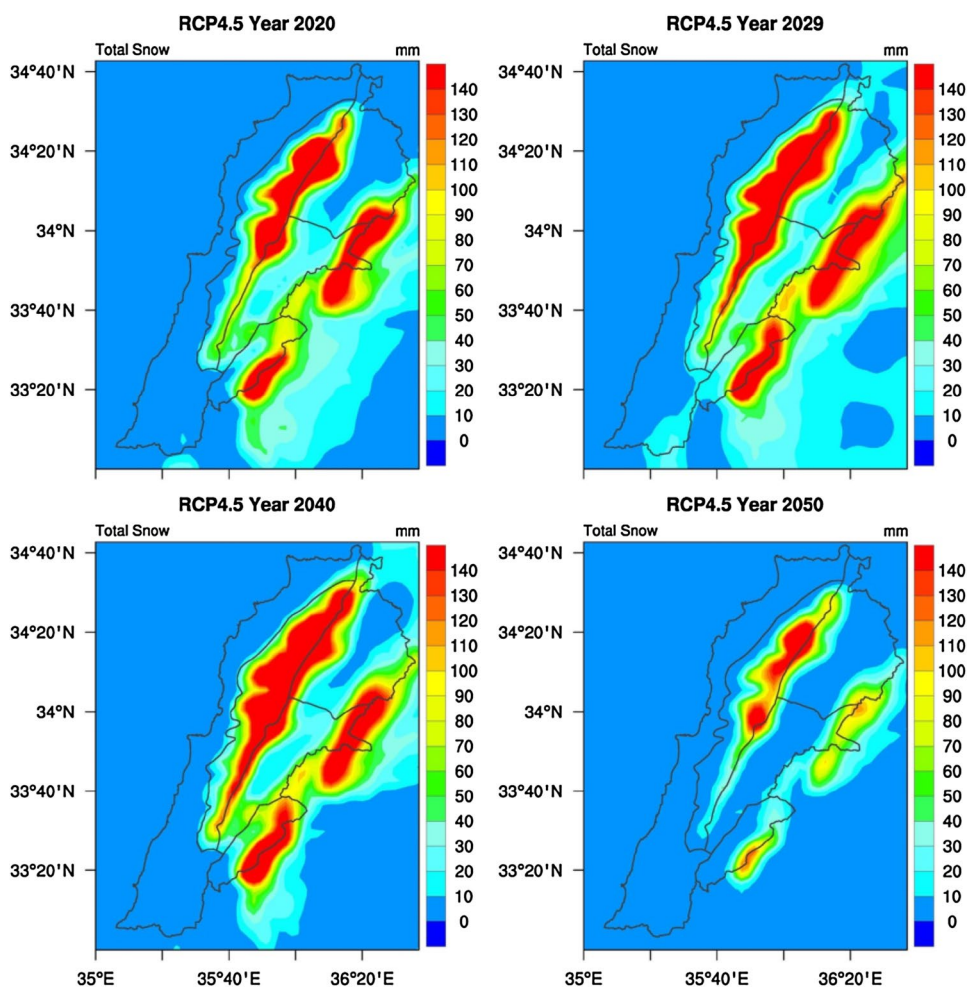
Moreover, the weather stations offer point records, whereas the model outputs are derived from a 3×3 km grid cell.

3.2 Future years (2011–2050)

The projected variations in the total annual precipitation (rain and snow) by HiRAM and WRF are presented in Table 2 and Figs. 9, 10, 11 and 12. All simulations predict a considerable decrease in annual precipitation in the selected simulated extreme years during the period 2011–2050, in comparison with present extreme hot and dry conditions (2008). Each year has the highest anomaly score in its decade (except 2020 and 2017 which were selected from a 5-year span between 2016 and 2020 as explained earlier); these reductions hence underline a worsening of the "worst-case" year in each decade in the future and consequently increasingly adverse impacts on the water resources of the region. Of particular concern is the potential for a 50% reduction in snowfall (RCP 4.5 year 2050) since snowmelt is a critical source of water recharge in the spring and early summer for the region.

The country averaged results alone are not sufficient to relay the whole scope of the impacts; regional changes should equally be examined. Precipitation changes in the selected simulated extreme years during the period 2011–2050 include a variable decrease across the different climatic zones (Table 3), which is in accordance with the results of Lelieveld et al. (2014) and IPCC (2013) for the Mediterranean region. Apart from 2017 to 2020, which represent poorly the extreme conditions in their respective decades since there were selected from 5 years only (particularly 2017 which is very wet), both RCPs produce a noticeable decrease in extreme years' rainy-season (October–May) rainfall. The reduction is substantial over all climatic sub-regions, but regional differences clearly arise. This is one of the main benefits of downscaling with RCMs WRF: their high spatial resolution allows the identification of regions and watersheds inside a study area that might be particularly exposed to future changes. To be specific, the mountainous areas in this study are likely to be affected by severe changes, where rainfall is expected to decrease by approximately 16 to 33% in RCP4.5, and 14 to 24% in

Fig. 11 RCP8.5 accumulated rainy-season rainfall (mm) for the extreme years (hottest and driest per decade) under consideration
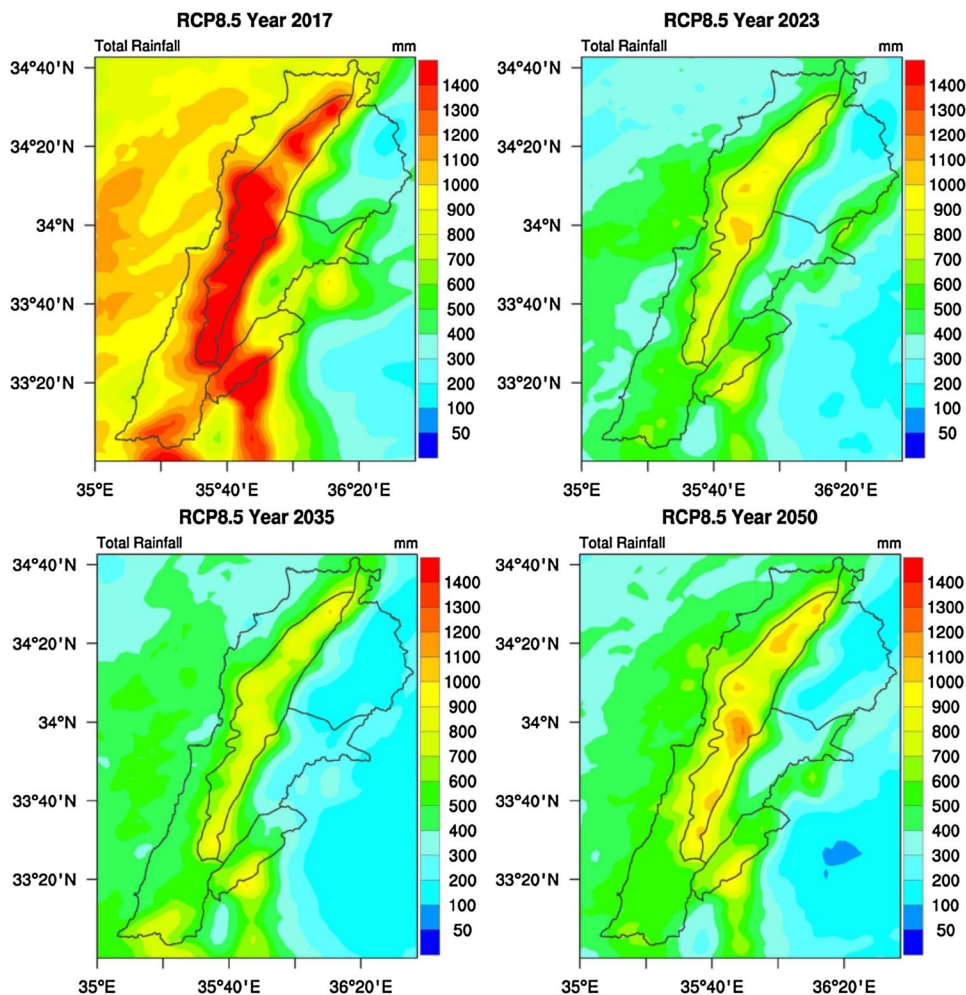
Fig. 12 RCP8.5 accumulated rainy-season snowfall (mm) for the extreme years (hottest and driest per decade) under consideration
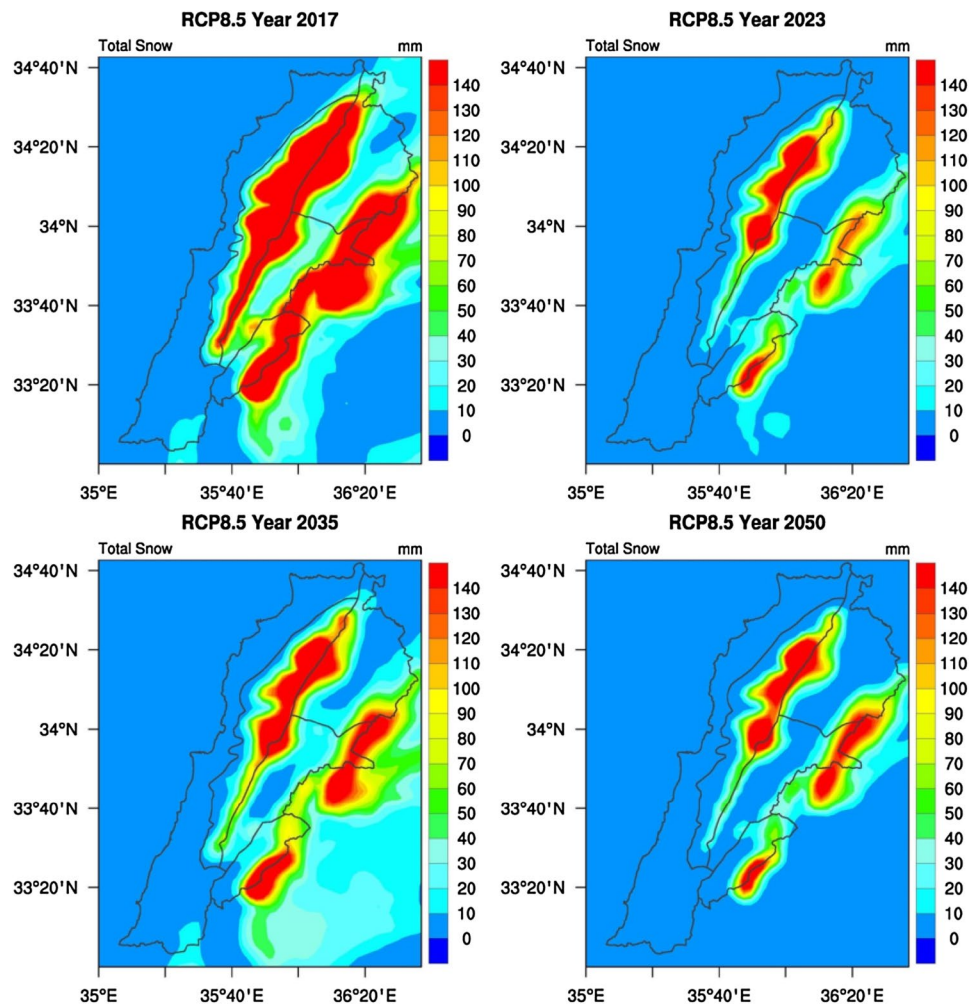

Table 3 Regional rainy-season rainfall and snowfall (mm) for RCP4.5 and 8.5

| Region	Reference	RCP4.5				RCP8.5			
	2008	2020	2029	2040	2050	2017	2023	2035	2050
Rainfall									
Coast	683	829	558	484	478	1098	519	537	601
Mountains	952	1032	803	636	735	1433	820	721	867
Inland_n	389	341	260	178	315	413	333	223	265
Inland_c	545	538	443	323	346	824	455	354	465
Inland_s	738	677	590	530	474	1155	584	520	618
Study area	**662**	**684**	**531**	**430**	**470**	**985**	**542**	**471**	**563**
Snowfall									
Coast	3	1	5	5	0	4	0	2	0
Mountains	95	121	135	156	61	249	73	91	66
Inland_n	34	38	53	45	16	88	23	36	25
Inland_c	57	58	64	63	16	110	26	44	28
Inland_s	54	67	88	91	21	131	37	59	33
Study area	**48**	**57**	**69**	**72**	**23**	**116**	**32**	**46**	**30**

Averages over the study area are shown in bold

RCP8.5, in comparison to 2008. Precipitation in the mountainous regions nourishes the highly productive agricultural interior areas and coastal zones, and future changes will affect food production due to water shortage. Furthermore, snowfall and subsequent slow snowmelt in the mountains smooth the water recharge, and reduction in snow accumulation can further adversely influence the study area. All simulations consistently locate significant precipitation decreases along the coast (between 12 and 30%), but the most notable changes are projected for the inland regions, especially in the northern area (15 to 54% decrease) with respect to the baseline year 2008. The worst decrease over the four extreme years in rainy-season rainfall in RCP4.5 (−35%) is more pronounced than in RCP8.5 (−29%) with respect to the extreme past dry year 2008. As for snowfall, it is likely to be impacted by climate warming with increases in saturation vapor pressures and fluctuations in the frequency of occurrence of temperatures below the

rain-snow shift temperature (O'Gorman 2015). Both RCPs predict an increase during the simulated extreme years from 2020 till 2040, but this is dissipated by the middle of the century and gives way to a decrease of about 36% over the mountains and exceeding 50% in the inland regions (the largest reduction in snowfall).

The probability density function (PDF) of daily rainfall allows the determination of the nature of potential changes, distinguishing the sort of events that might substantially vary, and outlining the precipitation patterns in the future. Figures 13 and 14 present the variations in the intensity and frequency of daily events in the 5 geo-climatic regions in RCP4.5 and 8.5 respectively, where only wet days ($P \geq 0.1$ mm/day) in the rainy-season are considered. The bins of PDF show the days of light rainfall ($P < 1$ mm/day), days of moderate rainfall (1 mm/day $\leq P \leq 10$ mm/day), days of heavy rainfall (10 mm/day $\leq P \leq 20$ mm/day) and very heavy rainfall ($P \geq 20$ mm/day). The PDFs show

**Fig. 13** Precipitation probability density plots per region in RCP4.5
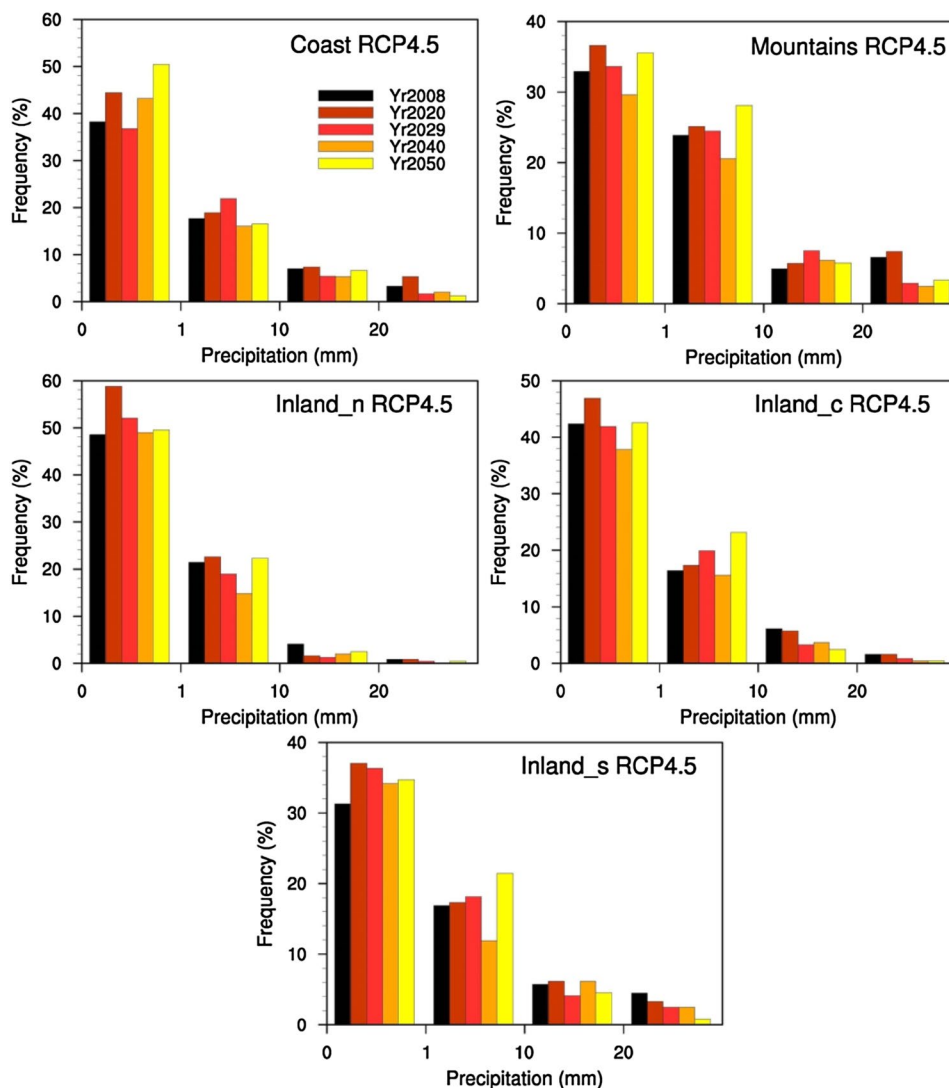
that there is generally a shift towards lower intensity events in all regions in both RCPs. The number of moderate rainfall events is projected to increase along the coast and in the mountainous region under both RCPs. As for the frequency of heavy precipitation, the simulated extreme years in RCP8.5 show a higher frequency of these rainfall events than those in RCP4.5 along the coast, as well as in the central and southern inland area.

The risk of extreme rainfall events and droughts, was further examined using five indices from the Expert Team on Climate Change Detection and Indices (ETCCDI) to portray changes in extreme precipitation: the number of consecutive dry days (CDD), consecutive wet days (CWD), days of heavy rainfall (R10MM), days of very heavy rainfall (R20MM) and maximum 1 day precipitation (RX1DAY) on a yearly basis (Persson et al. 2007) (Table 4). According to ETCCDI, CDD is the count, using the time series of daily precipitation amounts, of the largest number of consecutive days where rainfall rate is less than 1 mm/day. On the other hand, CWD is the count, using the time series of daily precipitation amounts, of the largest number of consecutive days where rainfall rate is at least 1 mm/day. Days of heavy rainfall is the count of days where the rainfall rate is greater than 10 mm, while days of very heavy rainfall is the number of days exceeding the rainfall rate of 20 mm. The maximum 1 day precipitation reports the highest rainfall rate attained during a day over the year. During the future simulated extreme years, the wet episodes are anticipated to be smaller, while the dry episodes are expected to be longer. The changes in CDD are more prominent in RCP4.5 than RCP8.5 in the simulated extreme years during the period 2011–2050. The worst year in RCP4.5 (2040) indicates that the length of the dry spells is likely to increase over the region, especially in the coast (58%), mountains (75%) and northern inland region (37%). The modifications in CWD suggest that the

Fig. 14 Precipitation probability density plots per region in RCP8.5
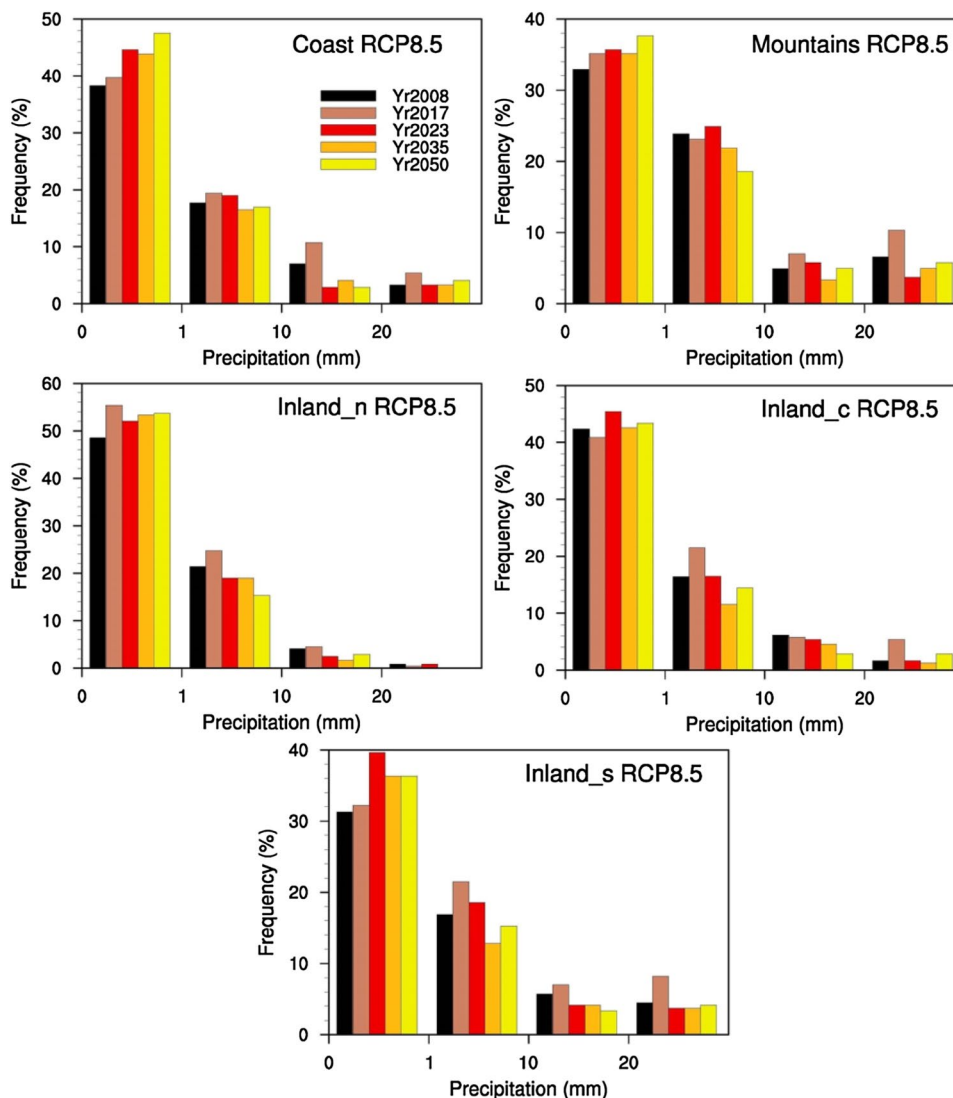
span of continuous wet periods during the future simulated extreme years is expected to decrease over practically the entire study area. The most substantial change is expected in the northern inland region under both RCPs where the CWD drops to 50% in the 2050 simulations. This is consistent with the findings of Barrera-Escoda et al. (2014) for the Iberian Peninsula who projected a decrease of 10 days in CDD and a reduction of 3–4 days in CWD in similar topographies in the Mediterranean region by year 2050. Hadjinicolaou et al. (2011) reported similar results for Cyprus by midcentury. Similarly, the number of days of heavy and very heavy rainfall (RR0MM and RR20MM) will decrease in the simulated future extreme years in most regions, reaching the level of 50% reduction in the northern inland zone already known for its dry climate, which is the same conclusion observed in that region's PDF (Figs. 13, 14). Finally, the maximum 1-day precipitation is expected to decrease in all regions under both scenarios during the extreme years except on the mountains, where WRF projected a slight increase. This result confirms the projections made for nearby Cyprus by 2050 (Hadjinicolaou et al. 2011), which is included in our outer domain of 9 km.

Table 4 Past and future CDD (days), CWD (days), RR10MM (days), RR20MM (days) and RX1day (mm) per region per RCP

Region	Reference	RCP4.5				RCP8.5			
	2008	2020	2029	2040	2050	2017	2023	2035	2050
CDD									
Coast	66	80	103	104	69	64	90	84	92
Mountains	65	85	98	114	67	73	82	80	69
Inland_n	100	109	120	137	71	114	124	125	110
Inland_c	121	114	126	135	83	117	122	102	122
Inland_s	111	110	130	119	79	109	120	100	111
Study area	**92**	**100**	**115**	**122**	**74**	**96**	**108**	**98**	**101**
CWD									
Coast	7	8	6	6	5	8	4	5	4
Mountains	8	8	6	6	6	8	6	6	5
Inland_n	6	6	4	4	4	6	5	4	3
Inland_c	6	7	5	5	5	7	5	5	5
Inland_s	7	8	5	5	6	8	5	6	5
Study area	**6**	**8**	**5**	**5**	**5**	**7**	**5**	**5**	**4**
RR10MM									
Coast	22	28	18	17	17	36	16	17	17
Mountains	28	33	25	20	24	41	25	21	24
Inland_n	12	9	7	5	9	36	16	17	17
Inland_c	18	18	13	10	10	41	25	21	24
Inland_s	23	23	18	17	16	12	10	6	8
Study area	**21**	**22**	**16**	**14**	**15**	**27**	**15**	**12**	**15**
RR20MM									
Coast	10	14	6	6	6	18	8	8	9
Mountains	15	18	12	9	10	24	11	12	13
Inland_n	4	3	2	1	3	4	3	2	2
Inland_c	7	7	5	3	3	12	6	5	7
Inland_s	10	10	7	8	9	12	9	8	10
Study area	**9**	**10**	**6**	**5**	**6**	**14**	**8**	**7**	**8**
RX1day									
Coast	62	57	74	46	42	74	51	54	64
Mountains	73	68	92	65	77	87	100	67	82
Inland_n	39	35	33	24	33	37	40	27	34
Inland_c	59	39	71	41	33	52	51	37	45
Inland_s	74	44	73	61	36	71	52	48	55
Study area	62	**49**	**69**	**47**	**44**	**64**	**59**	**47**	**56**

Averages over the study area are shown in bold

4 Summary and conclusion

In this study, the regional climate model WRF was used to downscale future climate simulated by the HiRAM GCM over a complex topographical area under the RCP4.5 and RCP8.5 scenarios. We simulated recent past extreme wet and dry years (2003 and 2008) and one future (2011–2050) extreme year per decade for each scenario: 2020, 2029, 2040 and 2050 from RCP4.5 and 2017, 2023, 2035 and 2050 from RCP8.5. Since the goal of this study is to compare the future driest year with the present driest year in order to determine how the extreme climate will shift, the baseline for comparison between the past and the future was the hottest/driest year 2008. Our focus being on water resources impacts, the selection of simulation years was performed using an anomaly score based on median annual temperature and accumulated precipitation from HiRAM daily time series. The higher inter-annual variability of precipitation resulted in it dominating this anomaly score. Model performance for average temperature and precipitation were evaluated by comparing the historic results for 2003 and 2008 results with decadal observations (2000–2010) for three weather stations located along the coast and in the central inland region. The historic results demonstrate that, compared with results from the coarse resolution of HiRAM, dynamical downscaling improves the simulated mean temperature and precipitation and is highly beneficial. The downscaled results were predominantly within the range of observed climatic ranges, correcting the cold bias inherited from HiRAM.

The improvement in temperature and precipitation obtained through downscaling are largely attributed to improvements in topography and coastline representation. WRF captured the severe distinction between the exceptionally wet climate on the seaward slopes of west mountain range, which is governed by orographic precipitation, and the dry climate inland. For such complex topographies, therefore, climate change impact assessment requires downscaling that can capture the strong spatial variability.

In the context of implications of the two scenarios RCP 4.5 and RCP8.5 on precipitation, the high-resolution downscaling simulations provided evidence of a significant drier climate over the whole study area during the simulated future extreme years from 2016 till the mid of this century, with reduction in annual precipitation of about 30%. The projections show that this significant decrease in precipitation spans all geo-climatic regions for both RCPs. However, nontrivial inter-regional differences, which can only be captured by high resolution RCMs, emerged. The mountainous areas as well as the inland regions will be particularly affected by these precipitation decreases (particularly in terms of snowfall), while the impacts in the coastal regions are slightly lower.

References

Akadan AR (2008). Climatic changes in Lebanon, predicting uncertain precipitation events—do climatic cycles exist? In Climatic changes and water resources in the Middle East and North Africa. (Eds) Zereini F, Hötz H. doi:10.1007/978-3-540-85047-2_6.

Antic S, Laprise R, Denis B, de Elia R (2004) Testing the downscaling ability of a one-way nested regional climate model in regions of complex topography. Clim Dyn 23:473–493. doi:10.1007/s00382-004-0438-5

Atlas Climatique du Liban (1977) Beyrouth: Republique libanaise Ministere des travaux publics et des transports, Direction de l'aviation civile

Bangalath HK, Stenchikov G (2015) Role of dust direct radiative effect on the tropical rain belt over Middle East and North Africa: a high-resolution AGCM study. J Geophy Res Atmos 120:4564–4584. doi:10.1002/2015JD023122

Barrera-Escoda A, Gonçalves M, Guerreiro D, Cunillera J, Baldasano JM (2014) Projections of temperature and precipitation extremes in the North Western Mediterranean basin by dynamical downscaling of climate scenarios at high resolution (1971–2050). Clim Change 122:567–582. doi:10.1007/s10584-013-1027-6

Bou-Zeid E, El-Fadel M (2002) Climate change and water resources in the Middle East: a vulnerability and adaptation assessment ASCE. J Water Res Plan Manag 128(5):343–355. doi:10.1061/(ASCE)0733-9496(2002)128:5(343)

Brown SJ, Caeser J, Ferro CAT (2008) Global changes in extreme daily temperature since 1950. J Geophy Res 113:D05115. doi:10.1029/2006JD008091

Bukovsky MS, Karoly DJ (2009) Precipitation simulations using WRF as a nested regional climate model. J Appl Meteorol Climatol 48(10):2152–2159. doi:10.1175/2009JAMC2186.1

Caldwell P, Chin HNS, Bader DC, Bala G (2009) Evaluation of a WRF dynamical downscaling simulation over California. Clim Change 95(3–4):499–521. doi:10.1007/s10584-009-9583-5

Cardoso RM, Soares PMM, Miranda PMA, Belo-Pereira M (2012) WRF high resolution simulation of Iberian mean and extreme precipitation climate. Int J Climatol 33(11):2591–2608. doi:10.1002/joc.3616

Chen F, Dudhia J (2001) Coupling an advanced land-surface hydrology model with the PennState NCAR MM5 modeling system. Part I: model description and implementation. Mon Weather Rev 129:569–585. http://journals.ametsoc.org/doi/abs/10.1175/1520-0493%282001%29129%3C0569%3ACAALSH%3E2.0.CO%3B2

Chen J, Lin S (2011) The remarkable predictability of inter-annual variability of Atlantic hurricanes during the past decade. Geophy Res Lett 38(11):L11804. doi:10.1029/2011GL047629/abstract

Christetin JH, Christenin OB (2007) A summary of the PRUDENCE model projections of changes in European climate by the end of this century. Clim Change 81:7–30. doi:10.1007/s10584-006-9210-7

Christidis N, Stott PA, Brown S, Hegerl GC, Cesars J (2005) Detection of changes in temperature extremes during the second half of the 20th century. Geophy Res Lett 32: L20716. doi:10.1029/2005GL023885.

Clarke L, Edmonds J, Jacoby H, Pitcher H, Reilly J, Richels R (2007) Scenarios of greenhouse gas emissions and atmospheric concentrations. Sub-report 2.1 A of Synthesis and assessment product 2.1 by the U.S. climate change science program and the subcommittee on global change research. Department of Energy, Office of Biological & Environmental Research, Washington, 7 DC., USA, pp 154. http://science.energy.gov/~/media/ber/pdf/Sap_2_1a_final_all.pdf

Collins W, Bellouin N, Woodward S et al (2011) Development and evaluation of an Earth-System model-HadGEM2. Geosci Model Dev 4(4):1051–1075. doi:10.5194/gmd-4-1051-2011

Delworth TL, Broccoli AJ, Rosati A, Stouffer RJ et al (2006) GFDL's CM2 global coupled climate models. Part I: formulation and simulation characteristics. J Clim 19(5):643–669, 672–674. http://journals.ametsoc.org/doi/abs/10.1175/JCLI3629.1

Diaz-Nieto J, Wilby RL (2005) A comparison of statistical downscaling and climate change factor methods: impacts on low flows in the River Thames, United Kingdom. Clim Change 69:245–268. doi:10.1007/s10584-005-1157-6

Donner LJ, Wyman BL, Hemler RS, Horowitz LW, Ming Y, Zhao M, Golaz JC, Ginoux P, Lin SJ, Schwarzkopf MD, Austin J, Alaka G, Cooke WF, Delworth TL, Freidenreich SM, Gordon CT, Griffies SM, Held IM, Hurlin WJ, Klein SA, Knutson TR, Langenhorst AR, Lee HC, Lin Y, Magi BI, Malyshev SL, Milly PCD, Naik V, Nath MJ, Pincus R, Ploshay JJ, Ramaswamy V, Seman CJ, Shevliakova E, Sirutis JJ, Stern WF, Stouffer RJ, Wilson RJ, Winton M, Wittenberg AT, Zeng F (2011) The dynamical core, physical parameterizations, and basic simulation characteristics of the atmospheric component AM3 of the GFDL global coupled model CM3. J Climate 24(13):3484–3519. doi:10.1175/2011JCLI3955.1

Dudhia J (1989) Numerical study of convection observed during the winter monsoon experiment using a mesoscale two-dimensional model. J Atmos Sci 46:3077–3107. doi:10.1175/1520-0469(1989)046<3077:NSOCOD>2.0.CO;2

El-Samra R (2016) High resolution dynamical downscaling to assess the impacts of climate change in regions of complex topography. PhD Dissertation, American University of Beirut, Lebanon

Evans J, McGregor J, McGuffie K (2012) Chap. 9—future regional climates. In: Henderson-Sellers Ann, McGuffie Kendal (eds) The future of the world's climate (second edition). Elsevier, Boston, pp 223–250. doi:10.1016/B978-0-12-386917-3.00009-9

Flaounas E, Drobinski P, Bastin S (2013a) Dynamical downscaling of IPSL-CM5 CMIP5 historical simulations over the Mediterranean: benefits on the representation of regional surface winds and cyclogenesis. Climate Dyn 40(9–10):2497–2513. doi:10.1007/s00382-012-1606-7

Flaounas E, Drobinski P, Vrac M, Bastin S, Lebeaupin-Brossier C, Stéfanon M, Borga M, Calvet JC (2013b) Precipitation and temperature space-time variability and extremes in the Mediterranean region: Evaluation of dynamical and statistical downscaling methods. Clim Dyn 40(11–12):2687–2705. doi:10.1007/s00382-012-1558-y

Fowler HJ, Blenkinsop S, Tebaldi C (2007) Linking climate change modelling to impacts studies: recent advances in downscaling techniques for hydrological modeling. Int J Climatol 27:1547–1578. doi:10.1002/joc.1556

Friedl MA, McIver DK, Zhang XY, Hodges JCF, Schnieder A, Bacinni A, Liu W (2001) Global land cover classification results from MODIS. In Geoscience and Remote Sensing Symposium, 2001. IGARSS'01. IEEE 2001 International (Vol. 2), 733–735. doi:10.1109/IGARSS.2001.976618

Gall JS, Ginis I, Lin SJ, Marchok TP, Chen JH (2011) Experimental tropical cyclone prediction using the GFDL 25-km-resolution global atmospheric model. Weather Forecast 26(6):1008–1019. doi:10.1175/WAF-D-10-05015.1

Gao Y, Fu JS, Drake JB, Liu Y, Lamarque JF (2012) Projected changes of extreme weather events in the eastern United States based on a high-resolution climate modelling system. Environ Res Lett 7(4):044025. doi:10.1088/1748-9326/7/4/044025

Gent PR, Danabasoqlu G, Donner LJ, Holland MM, Hunke EC et al (2011) The community climate system model version 4. J Clim 24:4973–4991. doi:10.1175/2011JCLI4083.1

Giorgi F, Mearns LO (1991) Approaches to the simulation of regional climate change: a review. Rev Geophys 29(2):191–216. doi:10.1029/90RG02636

Hadjinicolaou P, Giannakopoulos C, Zerefos C, Lange MA, Pashiardis S, Lelieveld J (2011) Mid-21st century climate and weather extremes in Cyprus as projected by six regional climate models. Reg Environ Change 11:441–457. doi:10.1007/s10113-010-0153-1

Heikkila U, Sandvik A, Sorteberg A (2011) Dynamical downscaling of ERA-40 in complex terrain using the WRF regional climate model. Clim Dyn 37(7–8):1551–1564. doi:10.1007/s00382-010-0928-6

Hong SY, Lim JOJ (2006) The WRF single-moment 6-class microphysics scheme (WSM6). J Korean Meteorol Soc 42(2):129–151. http://box.mmm.ucar.edu/wrf/users/docs/WSM6-hong_and_lim_JKMS.pdf. Accessed 11 Dec 2015

Intergovernmental Panel on Climate Change (IPCC) (2013) In: Stocker TF, Qin D, Plattner GK, Tignor M, Allen SK, Boschung J, Nauels A, Xia Y, Bex V Midgley PM (eds), Climate change 2013. The Physical Science Basis. Contribution of Working Group I to the Fifth Assessment Report of the Intergovernmental Panel on Climate Change. Cambridge University Press, Cambridge. http://www.ipcc.ch/report/ar5/wg1/

Janjic ZI (2001) Nonsingular implementation of the Mellor-Yamada level 2.5 scheme in the NCEP Meso model, Off. Note 437, 61 pp., National Centre for Environmental Protection, Boulder, Colorado. http://www.lib.ncep.noaa.gov/ncepofficenotes/files/on437.pdf. Accessed 14 Oct 2014

Jiang X, Waliser DE, Kim D, Zhao M, Sperber KR, Stern WF, Schubert SD, Zhang GJ, Wang W, Khairoutdinov M, Neale RB, Lee M (2012) Simulation of the intraseasonal variability over the eastern Pacific ITCZ in climate models. Clim Dyn 39(3):617–636. doi:10.1007/s00382-011-1098-x

Laprise R (2008) Regional climate modelling. J Comput Phys 227(7):3641–3666. doi:10.1016/j.jcp.2006.10.024

Lebeaupin Brossier C, Béranger K, Deltel C, Drobinski P (2011) The Mediterranean response to different space–time resolution atmospheric forcings using perpetual mode sensitivity simulations. Ocean Model 36(1–2):1–25. doi:10.1016/j.ocemod.2010.10.008

Lelieveld J, Hadjinicolaou P, Kostopoulou E, Giannakopoulos C, Pozzer A, Tanarhte M, Tyrlis E (2014) Model projected heat extremes and air pollution in the eastern Mediterranean and Middle East in the twenty-first century. Reg Environ Change 14:1937–1949. doi:10.1007/s10113-013-0444-4

Leung LR, Qian Y (2003) The sensitivity of precipitation and snowpack simulations to model resolution via nesting in regions of complex terrain. J Hydrometeorol 4:1025–1043. http://journals.ametsoc.org/doi/abs/10.1175/1525-7541(2003)004%3C1025%3ATSOPAS%3E2.0.CO%3B2

Li D, Bou-Zeid E, Baeck ML, Jessup S, Smith JA (2013) Modeling land surface processes and heavy rainfall in urban environments: Sensitivity to urban surface representations. J Hydrometeorol 14(4):1098–1118. doi:10.1175/JMH-D-12-0154.1

Lo JCF, Yang ZL, Pielke RA Sr (2008) Assessment of three dynamical climate downscaling methods using the weather research and forecasting (WRF) model. J Geophy Res Atmos 113(9):D09112. doi:10.1029/2007JD009216

Martin GM, Bellouin N, Derbyshire S et al (2011) The HadGEM2 family of Met Office Unified Model climate configurations. Geosci Model Dev 4:723–757. doi:10.5194/gmd-4-723-2011

Mellor GL, Yamada T (1974) A hierarchy of turbulence closure models for planetary boundary layers. J Atmos Sci 31:1791–1806. doi:10.1175/1520-0469(1974)031<1791:AHOTCM>2.0.CO;2

Mlawer EJ, Taubman SJ, Brown PD, Iacono MJ, Clough SA (1997) Radiative transfer for inhomogeneous atmosphere: RRTM, a validated correlated-k model for the longwave. J Geophys Res 102:16663–16682. doi:10.1029/97JD00237

O'Gorman PA (2015) Precipitation extremes under climate change. Curr Clim Change Rep 1:49–59. doi:10.1007/s40641-015-0009-3

Persson G, Bärring L, Kjellström E, Strandberg G, Rummukainen M (2007) Climate indices for vulnerability assessments. Swedish Meteorological and Hydrological Institute Meteorology and Climatology Rep. (RMK) 111, pp 80. http://www.smhi.se/polopoly_fs/1.805!Climate%20indices%20for%20vulnerability%20assessments.pdf

Qian Y, Ghan SJ, Leung LR (2010) Downscaling hydroclimatic changes over the western US based on CAM subgrid scheme and WRF regional climate simulations. Int J Climatol 30(5):675–693. doi:10.1002/joc.1928

Ramamurthy P, Li D, Bou-Zeid E (2015) High-resolution simulation of heatwave events in New York City. Theor Appl Climatol. doi:10.1007/s00704-015-1703-8.

Salathé E Jr, Steed R, Mass CF, Wilby PH (2008) A high-resolution climate model for the U.S. pacific northwest: mesoscale feedbacks and local responses to climate change. J Clim 21:5708–5726. doi:10.1175/2008JCLI2090.1

Seneviratne SI, Donat M, Mueller B, Alexander LV (2014) No pause in the increase of hot temperature extremes. Nature Clim Change 4:161–163. doi:10.1038/nclimate2145

Skamarock WC, Klemp JB, Dudhia J, Gill DO, Barker DM, Duda MG, Huang XY, Wang W, Powers JG (2008) A description of the Advanced Research WRF version 3, NCAR Tech. Note, NCAR/TN-475 + STR, pp 125, National Centre for Atmospheric Research, Boulder, Colorado. doi:10.5065/D6DZ069T

Soares PMM, Cardoso RM, Miranda PMA, de Medeiros J, Belo-Pereira M, Espirito-Santo F (2012) WRF high-resolution dynamical downscaling of ERA-interim for Portugal. Clim Dyn 39(9–10):2497–2522. doi:10.1007/s00382-012-1315-2

Sun Y, Solomon S, Dai A, Portmann RW (2007) How often will it rain? J Clim 20:4801–4818. doi:10.1175/JCLI4263.1

Talbot C, Bou-Zeid E, Smith J (2012) Nested mesoscale large-eddy simulations with WRF: performance in real test cases. J Hydrometeorol 13(5):1421–1441. doi:10.1175/JHM-D-11-048.1

Taylor KE, Stouffer RJ, Meehl GA (2012) An overview of CMIP5 and the experiment design. Bull Am Meteorol Soc 93:485–498. doi:10.1175/BAMS-D-11-00094.1

Volodin EM, Dianskii NA, Gusev AV (2010) Simulating present-day climate with the INMCM4.0 coupled model of the atmospheric and oceanic general circulations. Izv Atmos Ocean Phy 46:414–431. doi:10.1134/S000143381004002X

Wang Y, Leung LR, McGregor JL, Lee D, Wang WC, Ding Y, Kimura F (2004) Regional climate modeling: progress, challenges, and prospects. J Meteorol Soc Jpn 82(6):1599–1628. doi:10.2151/jmsj.82.1599

Warrach-Sagi K, Schwitalla T, Wulfmeyer V, Bauer H (2013) Evaluation of a climate simulation in Europe based on the WRF-NOAH model system: precipitation in Germany. Clim Dyn 41(3–4):755–774. doi:10.1007/s00382-013-1727-7

Wilby RL, Wigley TML, Conway D, Jones PD, Hewitson BC, Main J, Wilks DS (1998) Statistical downscaling of general circulation model output: a comparison of methods. Water Resour Res 34(11):2995–3008. doi:10.1029/98WR02577

Yukimoto S, Yoshimura H, Hosaka M et al. (2011) Meteorological research institute-earth system model v1 (MRI-ESM1)—model description. Technical Report of MRI. Ibaraki, Japan, pp 88. http://www.mri-jma.go.jp/Publish/Technical/DATA/VOL_64/tec_rep_mri_64.pdf

Zhang Y, Dulière V, Mote PW, Salathé EP (2009) Evaluation of WRF and HadRM mesoscale climate simulations over the U.S. Pacific Northwest. J Clim 22(20):5511–5526. doi:10.1175/2009JCLI2875.1

Zhao M, Held IM (2010) An analysis of the effect of global warming on the intensity of Atlantic hurricanes using a GCM with statistical refinement. J Clim 23(23):6382–6393. doi:10.1175/2010JCLI3837.1

Zhao M, Held IM, Lin SJ, Vecchi GA (2009) Simulations of global hurricane climatology, interannual variability, and response to global warming using a 50 km resolution GCM. J Clim 22:6653–6678. 10.1175/2009JCLI3049.1

Zhao M, Held IM, Vecchi GA (2010) Retrospective forecasts of the hurricane season using a global atmospheric model assuming persistence of SST anomalies. Mon Weather Rev 138:3858–3868. doi:10.1175/2010MWR3366.1